University of Texas Rio Grande Valley

ScholarWorks @ UTRGV

Civil Engineering Faculty Publications and Presentations

College of Engineering and Computer Science

2022

Concentration of fecal coliforms in marine waters using satellite images in the vicinity of Pucusana. Bay, Peru.

Y A. Palma-Gongora

F V. Zuta-Medina

Luis Angel Gomez-Cunya

Follow this and additional works at: https://scholarworks.utrgv.edu/ce_fac

 Part of the Civil Engineering Commons

PAPER • **OPEN ACCESS**

Concentration of fecal coliforms in marine waters using satellite images in the vicinity of Pucusana. Bay, Peru.

To cite this article: Y-A Palma-Gongora *et al* 2022 *IOP Conf. Ser.: Earth Environ. Sci.* **1077** 012005

View the article online for updates and enhancements.

You may also like

- A global, spatially-explicit assessment of irrigated croplands influenced by urban wastewater flows
A L Thebo, P Drechsel, E F Lambin et al.
- Spatial distribution of coliform bacteria in Batang Arau River, Padang, West Sumatera, Indonesia
D. Helard, S Indah and M Wilandari
- Bottled water quality and associated health outcomes: a systematic review and meta-analysis of 20 years of published data from China
Alasdair Cohen, Jingyi Cui, Qingyang Song et al.

This content was downloaded from IP address 129.113.53.71 on 11/10/2022 at 16:59

Concentration of fecal coliforms in marine waters using satellite images in the vicinity of Pucusana. Bay, Peru.

Y-A Palma-Gongora[1], F-V Zuta-Medina[1] and L-A Gomez-Cunya[1]

[1] School of Civil engineering, Peruvian University of Applied Sciences, Av. Prolongación Primavera 2390, Santiago de Surco, Lima, Perú

E-mail: u201622796@upc.edu.pe, u201622796@upc.edu.pe, pccilgom@upc.edu.pe

Abstract. Water quality monitoring in coastal areas is challenging due to cost and time constraints. Identifying and selecting sampling sites accurately and effectively is crucial for efficient monitoring. The need for efficient monitoring of marine waters has led to exploring the use of remote sensing as one helpful alternative. Remote sensing is practical in several applications based on pattern recognition and information processing of large terrestrial and aquatic surface areas. Collected information is processed with various image processing techniques to identify objects such as microorganisms. Fecal coliforms are microorganisms that are indicators of sanitary quality and are present in human and animal wastes discharged into water bodies reaching coastal regions. The present study estimated the presence of fecal coliforms as an indicator of contamination in coastal marine waters. Satellite data from two sensors, Landsat 7 ETM+ and Landsat 8 OLI, were used to evaluate the reflectance of fecal coliforms in marine waters. Then, statistical analysis and four regression models were tested to establish a functional correlation between the spectral bands and historical in situ fecal coliform measurement. In this research, satellite imagery in the vicinity of Pucusana Bay helped estimate the concentration of fecal coliforms in marine waters. As a result, a significant relationship was found between the shortwave infrared band splitting (SWIR 2) with the blue band and fecal coliforms presence. The relationship was used to estimate coliform concentration from the reflectance of the aquatic surface in Pucusana Bay. Finally, spatial distribution maps of fecal coliform concentrations were generated to compare the increase of these microorganisms over different years in the area. The methodology and results can be calibrated to other water body locations where fecal coliform is a concern.

1. Introduction

Lately, there have been efforts to integrate satellite data and in-situ measurements into long-term water quality monitoring in coastal areas [1] [2]. For instance, a robust correlation was found between satellite retrieved chlorophyll measurements and in situ measurements [3]. The presence of coliforms is familiar in soil and surface water. Human and animal wastewater can contain large quantities of certain types of coliform bacteria. Most coliform bacteria are harmless to humans, but others can cause severe waterborne diseases [4]. The presence of coliform is an issue in coastal areas due to human activities' uncontrolled disposal of wastewater and pollutants on the coast [5].

Content from this work may be used under the terms of the Creative Commons Attribution 3.0 licence. Any further distribution of this work must maintain attribution to the author(s) and the title of the work, journal citation and DOI.
Published under licence by IOP Publishing Ltd

Research is being conducted to estimate water pollution using remote sensing. For example, from satellite data and mathematical models, spatial distribution maps of the Ismailia channel in Egypt were created. These showed high pollution of drains due to effluent discharge from sewage treatment plants [6]. Similarly, a practical algorithm was developed with remotely sensed reflectances to estimate water surface chlorophyll for the Basque coastal waters of the Bay of Biscay [7]. Also, time series of multisensor satellite images are being incorporated to recover the diurnal variation of water constituent concentrations in coastal areas, serving as a warning for water quality management [8].

Big cities are a source of a considerable amount of wastewater, which can sometimes pollute coastal waters. For example, each inhabitant generates 145 liters of wastewater per day in Lima. This amount represents 1202286 m3 per day of sewage waste to the sewage system. From this amount, only 21.2% of the wastewater is treated. So, a considerable amount of sewage directly discharges into the sea [9]. There can also be other sources of pollution, such as seafood farming [10]

The main objective of this study is to estimate fecal coliform presence in coastal waters of the Pucusana Bay in Peru by calibrating a regression model using satellite data and in-situ measurements. So, satellite data from two sensors, Landsat 7 ETM+ and Landsat 8 OLI, were used in this study. Then, statistical analysis and four regression models were tested to establish a functional correlation between the spectral bands and historical in situ fecal coliform measurement. Next, the best-fit regression model was used to estimate coliform concentration from the reflectance of the aquatic surface in Pucusana Bay. Finally, spatial distribution maps of fecal coliform concentrations were generated to compare the increase of these microorganisms over different years in the area.

2. Methodology

2.1 Study area

Pucusana Bay (Figure 1) is near Lima, Peru, South America (UTM: 306036 East, 8619223 South). It has a maximum temperature of 26°C (79°F) and a minimum temperature of 15°C (59°F). The average wind speed is 15.6 km/h [11].

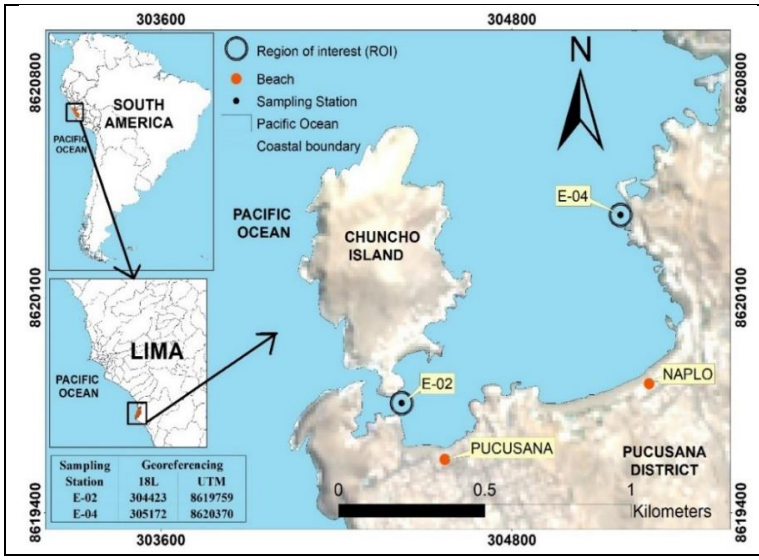

Figure 1 Study area near Pucusana Bay - Lima. It shows fecal coliform data and sampling locations.

Pucusana has an annual population growth rate of 3.4% (INEI, 2018), and its main economic activity is fishing and tourism [13] (Figure 2).

Figure 2 View of Pucusana bay showing fishing and tourist activity.

Pucusana and its neighbor beach Naplo have been classified as unhealthy for swimmers since 2016 [14]. They frequently present coliform concentration peaks of 1600 MPN/100ml or higher, exceeding the tolerable yearly limits. The direct discharge of domestic wastewater in the vicinity of the Bay is one of the leading causes of contamination. This pollution is a significant health issue because high concentrations of harmful bacteria and microorganisms in marine water can cause severe human illness [15].

2.2 Fecal coliform Data

Researchers collected on-site data from fecal coliform sample records from the environmental statistics yearbooks of the National Institute of Statistics and Informatics. The information on in-situ measurements in Pucusana Bay ranged from 2010 to 2019. Fecal coliform data have been collected from 2 stations (E-02 and E-04) [16] near the Bay (Figure 1). The measurement frequency is weekly during the southern hemisphere's summer, from December to April 15. The winter season measurements were biweekly from April 16 to November [17]. The sample records were sorted to match this study's satellite image date. From them, 22 satellite data matched in-situ measurement dates and were selected to continue with the analysis.

2.3 Satellite data, preprocessing, spectral signatures, band ratio, and statistical analysis

Landsat 7 ETM+ and Lansat 8 OLI satellite data from the study area were downloaded from the United States Geological Survey (USGS). The images with less than 10% cloud cover were selected because the climate and seasonal changes influence the relationship between water quality parameters and reflectance [18]. Therefore, researchers used summer data covering the first 18 weeks of each year from 2010 to 2019.

The preprocessing started with the atmospheric correction using the SCP (Semiautomatic Classification Plugin) of the QGIS software. This Geographic Information System GIS method uses the dark object subtraction method (DOS1). Any of the following formulas can obtain the radiance depending on the metadata of the selected image (equations 1, 2, and 3) [20]

$$L = \frac{DN - offset}{gain_2} \quad (1)$$

$$L = G_{rescale} DN + B_{rescale} \quad (2)$$

$$L = \left(\frac{L_{max} - L_{min}}{DN_{max} - DN_{min}}\right) \times (DN - DN_{min} + L_{min}) \quad (3)$$

Where L= radiance; and DN= Digital Numbers.

The SCP add-on transformed the digital values of satellite images into physical reflectance quantities by considering the pixel brightness value and error factors due to sensor malfunction or environmental distortion [20]. Next, radiometric and geometric corrections improved the spatial, temporal, and spectral parameters. The results analysis described surface radiation [21]

After finishing the preprocessing, we generated 22 satellite images' spectral signatures and the reflectance values of the regions of interest (ROI in Figure 1). Table 1 shows the reflectance for bands 1 to 7 of the 22 processed satellite data.

Table 1. Reflectance per band of satellite data matching in-situ measurement dates

No	Coliform in-situ measurements	Satellite data						
		Bands						
	MPN/100ml	b1	b2	b3	b4	b5	b6	b7
1	1600	-	0.036	0.042	0.052	0.059	0.078	0.057
2	920	0.017	0.019	0.019	0.023	0.029	0.031	0.026
3	920	0.038	0.040	0.041	0.047	0.052	0.055	0.047
4	920	-	0.017	0.020	0.024	0.022	0.019	0.020
5	900	-	0.032	0.036	0.043	0.042	0.042	0.030
6	540	0.027	0.031	0.036	0.041	0.050	0.044	0.031
7	540	0.044	0.045	0.051	0.054	0.061	0.055	0.050
8	540	0.015	0.017	0.021	0.025	0.024	0.023	0.020
9	540	0.020	0.024	0.028	0.032	0.033	0.035	0.031
10	490	-	0.021	0.024	0.029	0.030	0.031	0.025
11	350	0.031	0.034	0.037	0.042	0.050	0.049	0.043
12	350	-	0.028	0.033	0.037	0.037	0.029	0.024
13	280	-	0.033	0.038	0.042	0.046	0.035	0.033
14	240	0.017	0.018	0.021	0.022	0.024	0.025	0.022
15	240	0.023	0.028	0.036	0.038	0.042	0.039	0.029
16	240	-	0.055	0.056	0.065	0.068	0.062	0.050
17	240	-	0.032	0.032	0.037	0.041	0.037	0.030
18	240	0.017	0.019	0.023	0.024	0.024	0.021	0.018
19	240	-	0.028	0.030	0.030	0.030	0.025	0.027
20	210	-	0.036	0.039	0.047	0.051	0.050	0.042
21	170	0.028	0.033	0.038	0.032	0.027	0.025	0.021
22	130	0.017	0.018	0.023	0.022	0.021	0.020	0.018

The coastal aerosol band (Band 1) is only presented in Landsat 8 OLI images. Most of the analyzed satellite images are from Landsat 7 ETM+ and do not have the reflectance value in the aerosol band. Thus, some band ratios cannot be calculated and are presented with a dash in Tables 1 and 2. Once we obtained each band's reflectance values, band ratios (Table 2) were calculated to analyze their magnitude differences [22].

Table 2. Band ratio of satellite data matching in-situ measurement dates.

Band	Ratios in matching dates						
ratios	1	2	3	…	20	21	22
b1/b2	-	0.908	0.946	…	-	0.864	0.958

b1/b3	-	0.908	0.913	…	-	0.740	0.753
b1/b4	-	0.753	0.806	…	-	0.894	0.759
b1/b5	-	0.586	0.723	…	-	1.031	0.808
b1/b7	-	0.664	0.808	…	-	1.342	0.950
b2/b1	-	1.101	1.057	…	-	1.157	1.044
b2/b3	0.859	0.999	0.965	…	0.916	0.856	0.786
b2/b4	0.686	0.829	0.852	…	0.759	1.035	0.793
b2/b5	0.611	0.645	0.764	…	0.696	1.192	0.843
b2/b7	0.624	0.731	0.855	…	0.862	1.552	0.992
b3/b1	0.000	1.101	1.095	…	0.000	1.352	1.328
b3/b2	1.164	1.001	1.036	…	1.091	1.169	1.273
b3/b4	0.798	0.829	0.883	…	0.828	1.209	1.009
.	.	.	.	…	.	.	.
.	.	.	.	…	.	.	.
.	.	.	.	…	.	.	.
b7/b1	0.000	1.506	1.237	…	0.000	0.745	1.053
b7/b2	1.603	1.368	1.170	…	1.160	0.644	1.008
b7/b3	1.377	1.368	1.129	…	1.064	0.551	0.792
b7/b4	1.099	1.134	0.997	…	0.881	0.666	0.799
b7/b5	0.979	0.883	0.894	…	0.807	0.768	0.851
b7/b6	0.732	0.827	0.853	…	0.837	0.842	0.919
b1/b6	-	0.549	0.689	…	-	1.130	0.873
b2/b6	0.457	0.605	0.729	…	0.722	1.307	0.912
b3/b6	0.532	0.605	0.755	…	0.787	1.528	1.160
b4/b6	0.666	0.729	0.855	…	0.950	1.263	1.150
b5/b6	0.748	0.938	0.954	…	1.037	1.096	1.081
b6/b5	1.337	1.067	1.048	…	0.964	0.912	0.925

Four regression models were applied (linear, quadratic, logarithmic, and exponential) to study the relationship between fecal coliform samples (dependent variable) and the band ratios (independent variable). The relationships were measured using Karl Pearson's correlation coefficient (r in Equation (4)) [23].

$$r = \frac{\sum_{i=1}^{n}(Xi-\bar{X})(Yi-\bar{Y})}{\sqrt{[\sum_{i=1}^{n}(Xi-\bar{X})^2][\sum_{i=1}^{n}(Yi-\bar{Y})^2]}} \quad (4)$$

Finally, the best-fit regression model was used to generate maps of fecal coliforms in Pucusana Bay surroundings according to available satellite data.

3. Results

3.1 Statistical analysis of correlation (r)

The relationships between the reflectance values and the in-situ measurements were measured using Karl Pearson's correlation coefficient. The results are shown in Table 3. The first row shows each band, and the next row shows its correlation with the in-situ fecal coliform measurements. The subsequent rows show the band ratios and their correlation with the in-situ coliform measurements. The highest correlation coefficient has an "r" of 0.61 and corresponds to the band ratio b7/b2. SWIR 2 (2.1- 2.3 microns) is band 7 for Landsat 8 OLI and Lansat 7 ETM+. The blue band (0.45 - 0.515 microns) is band 2 on Landsat 8 OLI, and it is band 1 on Landsat 7 ETM+ [19].

Table 3 Pearson's Correlation coefficient of the relationships between the reflectance values and the in-situ measurements of fecal coliform.

Band	b1	b2	b3	b4	b5	b6	b7
r	0.31	0.16	0.22	0.36	0.36	0.52	0.51
Band ratio	b1/b2	b1/b3	b1/b4	b1/b5	b1/b7	b2/b1	b2/b3
r	0.11	0.13	-0.34	-0.47	-0.49	-0.11	-0.17
Band ratio	b2/b4	b2/b5	b2/b7	b3/b1	b3/b2	b3/b4	b3/b5
r	-0.55	-0.47	-0.52	-0.10	0.15	-0.48	-0.40
Band ratio	b3/b7	b4/b1	b4/b2	b4/b3	b4/b5	b4/b7	b5/b1
r	-0.49	0.34	0.58	0.51	-0.18	-0.35	0.49
Band ratio	b5/b2	b5/b3	b5/b4	b5/b7	b6/b1	b6/b2	b6/b3
r	0.48	0.39	0.17	-0.28	0.56	0.61	0.59
Band ratio	b6/b4	b6/b7	b7/b1	b7/b2	b7/b3	b7/b4	b7/b5
r	0.46	0.15	0.57	0.61(*)	0.57	0.41	0.29
Band ratio	b7/b6	b1/b6	b2/b6	b3/b6	b4/b6	b5/b6	b6/b5
r	-0.11	-0.34	-0.51	-0.50	-0.37	-0.38	0.44

3.2 Regresion model fit

The regression model was performed using the in-situ measurements of fecal coliform and the Band ratio with the highest correlation coefficient. The b7/b2 band ratio yielded the highest correlation coefficient and was selected for further analysis. Four regression models were applied (linear, quadratic, logarithmic, and exponential) to study the relationship between fecal coliform samples (dependent variable) and the b7/b2 band ratio (independent variable). The coefficient of determination (R^2) was calculated for each regression model. As a result, the exponential regression model (Figure 3) had an R^2 of 87% (Table 4) and was selected as the best-fit regression model (Equation (8)). Then, the prediction error of Equation 8 was calculated by subtracting the measured value and the predicted measured value in percentage (Table 5).

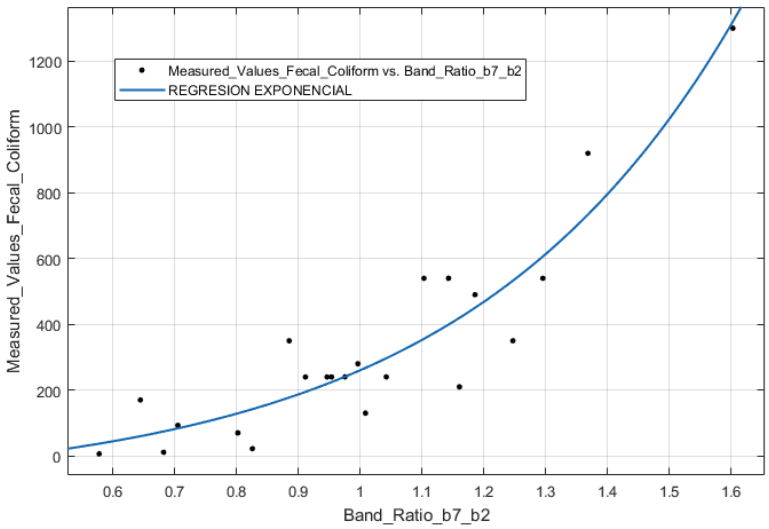

Figure 3 Exponential regression fit of the b7/b2 band ratio and the measured fecal coliform values.

Table 4 Regression model' equations of the b7/b2 band ratio and the measured fecal coliform values.

Regression	R^2 (%)	Equation	
Linear	75	1063X-737.1	(5)
Quadratic	86	126X^2-1579X+568	(6)
Logarithmic	33	845.5Log(X)+272.9	(7)
Exponential (*)	87	37.52Exp (2.268*X)-101.8	(8)

(*) Best-fit regression model

Where:

Y= Fecal coliform concentration (MPN/100ml) (most probable number per 100 mL)
X= b7/b2 band ratio reflectance.

Table 5 Prediction error of Equation 8 for estimating fecal coliform values (MPN/100ml).

N° Sample	Measured values	Predicted measured value from Equation (8)	Error (%)	N° Sample	Measured values	Predicted measured value from Equation (8)	Error (%)
1	1300	1321	-2%	23	130	233	-79%
2	920	734	20%	24	93	84	10%
3	920	614	33%	25	79	288	-265%
4	920	654	29%	26	79	304	-284%
5	900	838	7%	27	70	129	-85%
6	540	467	14%	28	33	321	-874%
7	540	489	9%	29	33	178	-440%
8	540	399	26%	30	30	240	-701%
9	540	607	-12%	31	22	142	-546%
10	490	450	8%	32	17	126	-640%
11	350	339	3%	33	11	74	-576%
12	350	343	2%	34	8	388	-4748%
13	280	257	8%	35	7	87	-1143%
14	240	203	15%	36	6	37	-520%
15	240	297	-24%	37	5	338	-6652%
16	240	195	19%	38	2	193	-9563%
17	240	219	9%	39	2	148	-7298%
18	240	241	0%	40	2	103	-5031%
19	240	224	6%	41	2	207	-10252%
20	210	227	-8%	42	2	28	-1276%
21	146	122	14%	43	2	111	-5455%
22	130	242	-86%				

Fecal coliform concentration estimation maps were obtained using the best-fit regression model (Equation 8) and GIS tools. The reflectance values of bands 2 (blue) and 7 (SWIR 2) in the satellite images of the Pucusana Bay were transformed using the regression model using the QGIS software. As a result, fecal coliform concentration estimation maps were obtained for different satellite images and dates. Color gradient quantified the distribution of fecal coliforms in the study area. As a result, the 2010 map (Figure 4) shows a low fecal coliform concentration near station E-02. Next, the 2015 map (Figure 5) presents an increase in the presence of fecal coliform in the

area. And in the 2021 map (Figure 6), higher fecal coliform concentrations existed near the Bay area. In-situ fecal coliform measurements are not publicly available to date yet. However, we were able to estimate those concentrations using satellite images indirectly.

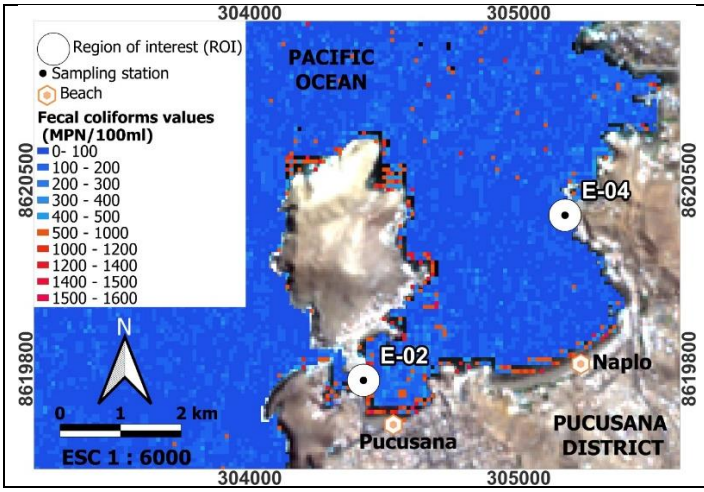

Figure 4 Estimated fecal coliforms in Pucusana Bay near Lima using Lansat 7 satellite image from February 8, 2010.

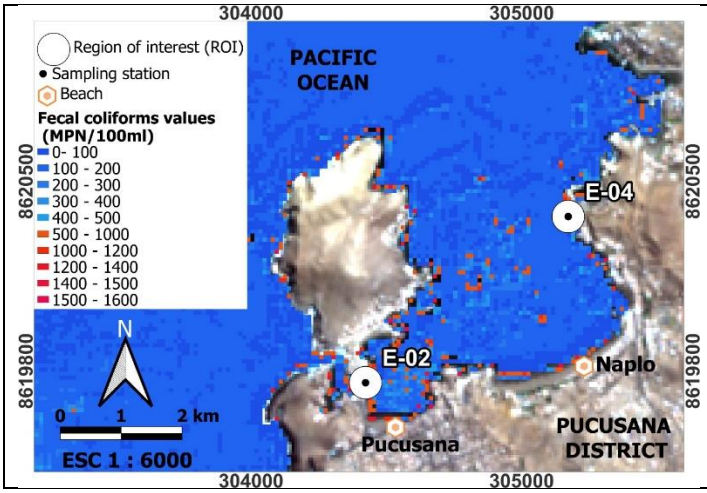

Figure 5 Estimated fecal coliforms in Pucusana Bay near Lima using Lansat 8 satellite image from January 29, 2015.

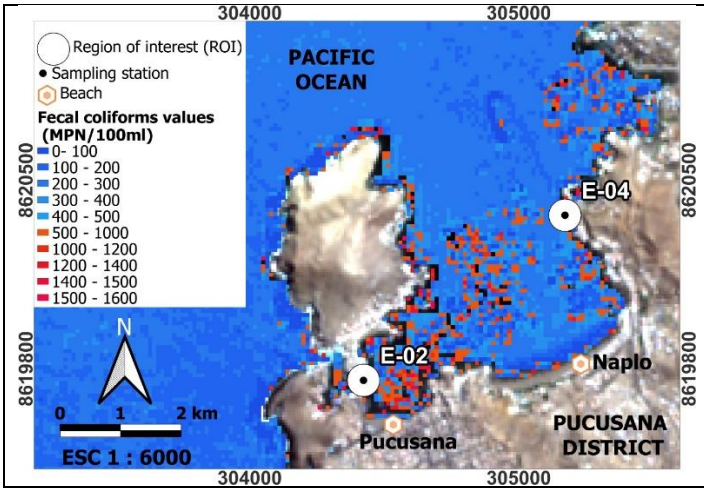

Figure 6 Estimated fecal coliforms in Pucusana Bay near Lima using Lansat 8 satellite image from March 18, 2021.

4. Discussion

For the Pucusana Bay and its surroundings, water is considered quality for primary recreational contact [25] when fecal coliforms are less than 200 MPN/100ml [26]. For secondary recreational contact (USEPA, 2012), fecal coliforms should not exceed 1000 MPN/100ml [26]. The results show that fecal coliform concentration between 2010 and 2021 has increased near the Pucusana Bay areas, which is worrisome. Current developments and the regression model (Equation (8)) can be used by health authorities to track in near-realtime the changes of fecal coliform in the Bay

The results showed that the regression model error decreased as the coliform concentration increased. It is noticed that the regression model error grows substantially for concentration values lower than 80 MPN/100ml. So, the regression model can be suitable for monitoring water quality exceeding primary or secondary recreational contact tolerances.

Since higher concentrations of fecal coliform had higher reflectance values, the high reflectance of shallow water can mislead the calculations and error increase. To prevent miscalculations and reduce errors, in this study, the analysis of the regression model restricted the reflectance values to lower than 1600 MPN/100ml. This limit coincides with the threshold values of the in-situ measurements data of fecal coliform [17].

5. Conclusions

The fecal coliform concentration has increased near the Pucusana Bay areas in the last decade. Some causes can be urban growth, direct wastewater discharge, inefficient sanitary systems, etc. The consequence of this pollution is the increase in health risks for users of the Bay. The results of this study can be used by health authorities to track the changes in fecal coliform in the Bay in near-real-time.

This study presented a functional method to estimate concentrations of fecal coliforms in coastal areas using publicly available satellite data. Implementing this methodology can be cost-effective for monitoring fecal coliform presence in coastal waters. Hence, it could help find locations where structural or non-structural remedies for sanitation are needed. Eventually, it will contribute to Pucusana Bay's population wellbeing. Therefore, Pucusana Bay should improve the water quality management of its coastal marine waters to reduce the consistent pollution increase shown by the regression model implemented in this study.

The present study achieved the goal of estimating concentrations of fecal coliforms (dependent variable) in coastal areas using publicly available satellite data (independent variable) and comparing four well-known regression models. Future work to improve the estimation of fecal coliforms values can include implementing other image processing techniques such as intelligent optimization techniques with fuzzy entropy [27], salp swarm algorithms [28], signal processing techniques for enhanced feature selection and higher classification accuracy [29], Aquila optimizer and arithmetic optimization algorithms [30], etc.

Acknowledgments

The authors acknowledge the support of the Department of Civil Engineering of the University of Applied Sciences, Perú.

References

[1] N. Kabbara, J. Benkhelil, M. Awad, and V. Barale, "Monitoring water quality in the coastal area of Tripoli (Lebanon) using high-resolution satellite data," *ISPRS Journal of Photogrammetry and Remote Sensing*, vol. 63, no. 5, pp. 488–495, Sep. 2008, doi: 10.1016/J.ISPRSJPRS.2008.01.004.

[2] B. Arabi, M. S. Salama, J. Pitarch, and W. Verhoef, "Integration of in-situ and multisensor satellite observations for long-term water quality monitoring in coastal areas," *Remote Sensing of Environment*, vol. 239, p. 111632, Mar. 2020, doi: 10.1016/j.rse.2020.111632.

[3] E. T. Harvey, S. Kratzer, and P. Philipson, "Satellite-based water quality monitoring for improved spatial and temporal retrieval of chlorophyll-a in coastal waters," *Remote Sensing of Environment*, vol. 158, pp. 417–430, Mar. 2015, doi: 10.1016/j.rse.2014.11.017.
[4] B. R. Swistock, S. Clemens, W. E. Sharpe, and S. Rummel, "Water quality and management of private drinking water wells in Pennsylvania," *Journal of Environmental Health*, vol. 75, no. 6, pp. 60–66, 2013.
[5] S. Tanahara *et al.*, "Spatial and temporal variations in water quality of Todos Santos Bay, northwestern Baja California, Mexico," *Marine Pollution Bulletin*, vol. 173, p. 113148, Dec. 2021, doi: 10.1016/j.marpolbul.2021.113148.
[6] M. El-Rawy, H. Fathi, and F. Abdalla, "Integration of remote sensing data and in situ measurements to monitor the water quality of the Ismailia Canal, Nile Delta, Egypt," *Environmental Geochemistry and Health*, vol. 42, no. 7, pp. 2101–2120, Jul. 2020, doi: 10.1007/s10653-019-00466-5.
[7] S. Novoa *et al.*, "Water quality monitoring in Basque coastal areas using local chlorophyll-a algorithm and MERIS images," *https://doi.org/10.1117/1.JRS.6.063519*, vol. 6, no. 1, p. 063519, Apr. 2012, doi: 10.1117/1.JRS.6.063519.
[8] B. Arabi, M. S. Salama, J. Pitarch, and W. Verhoef, "Integration of in-situ and multisensor satellite observations for long-term water quality monitoring in coastal areas," *Remote Sensing of Environment*, vol. 239, p. 111632, Mar. 2020, doi: 10.1016/j.rse.2020.111632.
[9] OEFA, "Fiscalización ambiental en aguas residuales.," *Organismo de Evaluacion y Fiscalizacion Ambiental*, p. 36, 2014, [Online]. Available: https://www.oefa.gob.pe/?wpfb_dl=7827
[10] T. D. Bui, J. Luong-Van, and C. M. Austin, "Impact of shrimp farm effluent on water quality in coastal areas of the world heritage-listed Ha Long Bay," *American Journal of Environmental Sciences*, vol. 8, no. 2, pp. 104–116, Mar. 2012, doi: 10.3844/ajessp.2012.104.116.
[11] "El clima en Pucusana, el tiempo por mes, temperatura promedio (Perú) - Weather Spark." https://es.weatherspark.com/y/21286/Clima-promedio-en-Pucusana-Per%C3%BA-durante-todo-el-a%C3%B1o#Figures-Temperature (accessed Mar. 07, 2022).
[12] INEI, "RESULTADOS DEFINITIVOS ," 2018.
[13] Jorge Amadeo Medicina Di Paolo, "El Sistema de turismo marino en el distrito de Pucusana, como gestión empresarial:," 2010.
[14] J. Inei, "Créditos," 2020.
[15] undefined Cloudfront, "Bacterias Coliformes," p. undefined-undefined, 2017.
[16] MINSA, "Vigilancia y Monitoreo de los Recursos Hídricos | DIGESA," 2006. http://www.digesa.minsa.gob.pe/DEPA/vigilancia_recursos_hidricos.asp (accessed Feb. 12, 2022).
[17] DIGESA, "Directiva Sanitaria que Establece el Procedimiento para la Evaluación de la Calidad Sanitaria de las Playas del Litoral Peruano ," 2011, Accessed: Feb. 12, 2022. [Online]. Available: www.digesa.minsa.gob.pe
[18] K. W. Abdelmalik, "Role of statistical remote sensing for Inland water quality parameters prediction," *Egyptian Journal of Remote Sensing and Space Science*, vol. 21, no. 2, pp. 193–200, Sep. 2018, doi: 10.1016/J.EJRS.2016.12.002.
[19] S. M. Kloiber, P. L. Brezonik, and M. E. Bauer, "Application of Landsat imagery to regional-scale assessments of lake clarity," *Water Research*, vol. 36, no. 17, pp. 4330–4340, 2002, doi: 10.1016/S0043-1354(02)00146-X.
[20] M. Gudelj, M. Gašparović, and M. Zrinjsk, "Accuracy analysis of the inland waters detection," *International Multidisciplinary Scientific GeoConference Surveying Geology and Mining Ecology Management, SGEM*, vol. 18, no. 1.5, pp. 203–210, 2018, doi: 10.5593/sgem2018v/1.5/s02.025.

[21] K. A. Galvin, R. B. Boone, N. M. Smith, and S. J. Lynn, "Impacts of climate variability on East African pastoralists: Linking social science and remote sensing," *Climate Research*, vol. 19, no. 2, pp. 161–172, 2001, doi: 10.3354/CR019161.
[22] M. H. Abd, "Water Quality Evaluation For River reach by using the Remote Sensing, AL-Gharraf River Southern Iraq as a case study.," *Engineering Technical College*, 2017, Accessed: February 14, 2022. [Online]. Available: https://www.researchgate.net/publication/326673570_Water_Quality_Evaluation_For_River_reach_by_using_the_Remote_Sensing_AL-Gharraf_River_Southern_Iraq_as_a_case_study
[23] S. Rewatkar, S. Doifode, and A. Kanojiya, "Correlation and linear regression analysis of water quality parameters of Wainganga River at Desaiganj (Wadsa) in Gadchiroli district Maharashtra, India," *International Journal of Academic Research and Development*, vol. 1, no. 9, pp. 39–44, Sep. 2016, Accessed: March 07, 2022. [Online]. Available: http://www.academicjournal.in/archives/2016/vol1/issue9/1-9-21
[24] Y. Chen, G. Liu, and H. Chen, "Multi-temporal remote sensing image registration based on multi-layer feature fusion of deep residual network," *ICIIBMS 2019 - 4th International Conference on Intelligent Informatics and Biomedical Sciences*, pp. 363–367, Nov. 2019, doi: 10.1109/ICIIBMS46890.2019.8991506.
[25] USEPA, "Water Quality Standards Handbook Chapter 2 : Designation of Uses," *EPA Office of Water, Office of Science and Technology, Washington, DC.*, no. EPA-832-B-12-002, p. 39, 2012.
[26] MINAM, “Decreto Supremo N° 002-2008-MINAM | Ministerio del Ambiente,” 2008.
[27] S. Mahajan, N. Mittal, and A. K. Pandit, "Image segmentation using multilevel thresholding based on type II fuzzy entropy and marine predators algorithm," *Multimedia Tools and Applications*, vol. 80, no. 13, pp. 19335–19359, May 2021, doi: 10.1007/S11042-021-10641-5/TABLES/5.
[28] S. Mahajan, N. Mittal, R. Salgotra, M. Masud, H. A. Alhumyani, and A. K. Pandit, "An Efficient Adaptive Salp Swarm Algorithm Using Type II Fuzzy Entropy for Multilevel Thresholding Image Segmentation," *Computational and Mathematical Methods in Medicine*, vol. 2022, 2022, doi: 10.1155/2022/2794326.
[29] S. Mahajan and A. K. Pandit, "Hybrid method to supervise feature selection using signal processing and complex algebra techniques," *Multimedia Tools and Applications 2021*, pp. 1–22, Oct. 2021, doi: 10.1007/S11042-021-11474-Y.
[30] S. Mahajan, L. Abualigah, A. K. Pandit, and M. Altalhi, "Hybrid Aquila optimizer with arithmetic optimization algorithm for global optimization tasks," *Soft Computing 2022*, pp. 1–19, Feb. 2022, doi: 10.1007/S00500-022-06873-8.